

Adaptive Parameter Control Using AAN for Lower Limb Rehabilitation Exoskeletons

Zheng Sun¹, Wenkong Wang¹, Zizhong Wei^{*2}, Xin Ma^{*1}

1. Center for Robotics, School of Control Science and Engineering,
Engineering Research Center of Intelligent Unmanned System, Ministry of Education,
Shandong University,
No.17923, Jingshi Road(s), Jinan, 250061, China

2. Shandong Inspur Science Research Institute Co., Ltd.

Abstract: Exoskeletons play a crucial role in assisting patients with varying mobility levels during rehabilitation. However, existing control strategies face challenges such as imprecise trajectory tracking, interaction torque oscillations, and limited adaptability to diverse patient conditions. To address these issues, this paper proposes an assist-as-needed (AAN) control algorithm that integrates a human-robot coupling dynamics model, a human torque-momentum observer (HTMO), and an adaptive parameter controller (APC). The algorithm first employs inverse dynamics to compute the joint torques required for the rehabilitation trajectory. The HTMO then estimates the torque exerted by the patient's joints and determines the torque error, which the exoskeleton compensates for via a spring-damper system, ultimately generating the target trajectory. Finally, the APC ensures adaptive assistive control. The proposed method is validated for its effectiveness in Matlab/Simulink.

Key Words: Human-machine coupling dynamics, Assist-as-needed control, Adaptive parameter controller

1 Introduction

Stroke is one of the leading causes of disability and death worldwide, with its incidence rising annually, especially in aging societies[1]. After a stroke, patients often experience hemiplegia and muscle weakness, which severely affect their quality of life. Traditional rehabilitation methods, primarily physical therapy, aid recovery but are limited by treatment intensity and duration. With the growing shortage of medical resources, exoskeleton-assisted rehabilitation has emerged as an innovative technology, demonstrating significant success in providing personalized and efficient rehabilitation support while helping patients recover motor function[2][3].

Exoskeleton-assisted rehabilitation therapy is categorized into passive and active modes. In the passive mode[4], the exoskeleton assists the patient in performing rehabilitation exercises without requiring active exertion, typically employed in the early stages of rehabilitation. In the active mode[5], the exoskeleton provides assistance through a power system, enabling the patient to actively exert force, thereby facilitating the recovery of muscle strength and motor coordination. By incorporating the AAN strategy, the exoskeleton can dynamically adjust the level of assistance based on the patient's real-time needs, offering precise support and avoiding both excessive and insufficient assistance, thus optimizing rehabilitation outcomes[6][7]. When evaluating the patient's movement ability, trajectory tracking error can serve as an indicator of recovery capacity; the smaller the error, the better the patient's movement ability[8].

In recent years, active control, particularly AAN control, has become a research hotspot in academia. Numerous studies have focused on acquiring human motion intentions using various approaches, such as force/torque sensors[9][10], electroencephalography (EEG)/electromyography (EMG) signals[11][12], and inertial measurement unit (IMU) sensors. Although these methods show some potential, they

still face some limitations in practical applications. For instance, force/torque sensors are expensive, require precise installation, and can constrain human-machine interactions. Similarly, EEG and EMG signals, though informative, suffer from low signal-to-noise ratios and susceptibility to interference, limiting their reliability in real-world settings.

To overcome these challenges, recent studies[7][13] have explored alternative strategies, such as motion intention observation based on interactive torque observers. These methods use techniques like Kalman filtering to mitigate modeling inaccuracies and improve estimation reliability. Despite these advances, the main problems with existing methods are as follows: 1) Many solutions rely on external sensors, which introduce complexity and increase system cost. 2) Existing approaches lack sufficient adaptability to accommodate individual user differences, leading to suboptimal performance across diverse users.

In comparison to the previous work this paper makes the following improvements:

1) A sensorless joint torque estimation method is introduced, which leverages system dynamics and real-time feedback, thereby eliminating the reliance on external sensors. This reduction in hardware complexity and cost is achieved without compromising the accuracy of torque estimation.

2) An adaptive control strategy is developed to address inter-user variability, ensuring robust performance across individuals with varying biomechanical characteristics. This enhances the system's versatility and reliability, thereby expanding its applicability to a diverse user population.

The structure of this paper is as follows: Section 2 describes the Human-machine coupled dynamics systems; In Section 3, the torque observer and the target controller are given; Simulation results and discussion are provided in Section 4; Section 5 provides a summary.

This work was supported in part by the National Key Research and Development Program (No. 2023YFB4706104).

2 Problem Formulation

2.1 Human/Exoskeleton model

The model in Fig. 1 (left) illustrates the rehabilitation exoskeleton, consisting of hip and knee joint modules and support straps. It assists hip and knee flexion/extension during gait rehabilitation, with control based on lower limb dynamics[15], as detailed below:

$$M_i(q_i)\ddot{q}_i + C_i(\dot{q}_i, q_i)\dot{q}_i + G_i(q_i) = \tau_i \quad i = h \text{ or } e \quad (1)$$

where $M_i(q_i)$ is the joint inertia matrix, $C_i(\dot{q}_i, q_i)$ represents coriolis matrix, $G_i(q_i)$ is the gravity matrix, and τ_i is the control input torque. q_i , \dot{q}_i , and \ddot{q}_i denote joint angle, angular velocity, and acceleration, respectively. i can be h (human) or e (exoskeleton), distinguishing their kinetic parameters. The expressions are given as:

$$\begin{aligned} M_i &= \begin{bmatrix} m_{i11} & m_{i12} \\ m_{i21} & m_{i22} \end{bmatrix}, C_i = \begin{bmatrix} c_{i11} & c_{i12} \\ c_{i21} & 0 \end{bmatrix}, \\ G_i &= [g_{i1} \quad g_{i2}]^T \end{aligned} \quad (2)$$

where $m_{i11} = m_{i2}L_{i1}^2 + 2m_{i2}C_{i2}L_{i1}l_{i2} + m_{i1}l_{i1}^2 + m_{i2}l_{i2}^2 + J_{i1} + J_{i2}$, $m_{i12} = m_{i21} = m_{i2}l_{i2}^2 + L_{i1}m_{i2}C_{i2}l_{i2} + J_{i2}$, $m_{i22} = m_{i2}l_{i2}^2 + J_{i2}$, $c_{i11} = -2L_{i1}l_{i2}m_{i2}S_{i2}\dot{\theta}_{i2}$, $c_{i12} = -L_{i1}l_{i2}m_{i2}S_{i2}\dot{\theta}_{i2}$, $L_{i1}l_{i2}m_{i2}S_{i2}\dot{\theta}_{i1}$, $G_{i1} = -gl_{i2}m_{i2}C_{i1}l_{i2} - L_{i1}gm_{i2}C_{i1} - gl_{i1}m_{i1}C_{i1}$, $G_{i2} = -gl_{i2}m_{i2}C_{i1}l_{i2}$. The variables $q_i = [\theta_{i1}, \theta_{i2}]^T$, $\dot{q}_i = [\dot{\theta}_{i1}, \dot{\theta}_{i2}]^T$, and $\ddot{q}_i = [\ddot{\theta}_{i1}, \ddot{\theta}_{i2}]^T$. The trigonometric terms like S_{ij} and C_{ij} denote $\sin(\theta_{ij})$ ($j = 1, 2$) and $\cos(\theta_{ij})$ ($j = 1, 2$), respectively. The complete notation definitions are given in **Table1**.

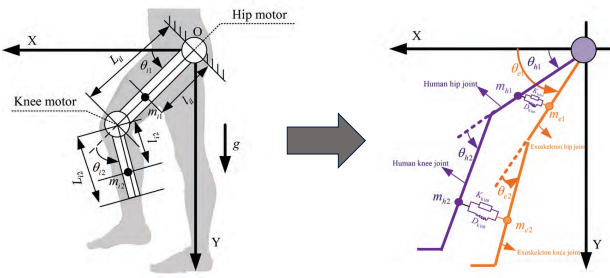


Fig. 1: Human-machine coupled dynamics system

2.2 Coupling model of interaction forces

As shown in Fig. 1 (right), the exoskeleton-human coupling is modeled using a spring-damping system, assuming aligned hip/knee joints connected by straps. The interaction torque is derived as follows[15]:

$$F_h = K_{\text{hint}} \begin{bmatrix} x_{e1} - x_{h1} \\ y_{e1} - y_{h1} \end{bmatrix} + D_{\text{hint}} \begin{bmatrix} \dot{x}_{e1} - \dot{x}_{h1} \\ \dot{y}_{e1} - \dot{y}_{h1} \end{bmatrix} \quad (3)$$

$$F_k = K_{\text{kint}} \begin{bmatrix} x_{e2} - x_{h2} \\ y_{e2} - y_{h2} \end{bmatrix} + D_{\text{kint}} \begin{bmatrix} \dot{x}_{e2} - \dot{x}_{h2} \\ \dot{y}_{e2} - \dot{y}_{h2} \end{bmatrix} \quad (4)$$

Where F_h and F_k represent the interaction forces at the hip and knee joints, respectively. K_{hint} and K_{kint} are the

Table 1: System parameters

Parameters	Physical meaning
L_{i1}	Length of thigh
l_{i1}	Length from hip to thigh center of mass
m_{i1}	Mass of thigh
J_{i1}	Hip joint moment of inertia
θ_{i1}	Hip rotation angle
L_{i2}	Length of shank
l_{i1}	Length from knee to thigh center of mass
m_{i2}	Mass of shank
θ_{i2}	Knee rotation angle
J_{i2}	Knee joint moment of inertia
g	Gravitational acceleration
K	System coupling stiffness
D	System coupling damping

stiffness parameters, while D_{hint} and D_{kint} are the damping parameters for the hip and knee joints. The coordinates of the centers of mass for the human thigh and shank, as well as the exoskeleton's thigh and shank, are denoted as $H_h(x_{h1}, y_{h1})$, $H_k(x_{h2}, y_{h2})$, $E_h(x_{e1}, y_{e1})$, and $E_k(x_{e2}, y_{e2})$, respectively. The specific expressions are as follows:

$$\begin{aligned} & \begin{cases} x_{i1} = l_{i1}S_{i1} \\ y_{i1} = l_{i1}C_{i1} \\ x_{i2} = L_{i1}S_{i1} + l_{i2}S_{i1i2} \\ y_{i2} = L_{i1}C_{i1} + l_{i2}C_{i1i2} \end{cases} \\ \Rightarrow & \begin{cases} \dot{x}_{i1} = l_{i1}C_{i1}\dot{\theta}_{i1} \\ \dot{y}_{i1} = -l_{i1}S_{i1}\dot{\theta}_{i1} \\ \dot{x}_{i2} = L_{i1}C_{i1}\dot{\theta}_{i1} + l_{i2}C_{i1i2}(\dot{\theta}_{i1} + \dot{\theta}_{i2}) \\ \dot{y}_{i2} = -L_{i1}S_{i1}\dot{\theta}_{i1} - l_{i2}S_{i1i2}(\dot{\theta}_{i1} + \dot{\theta}_{i2}) \end{cases} \quad (5) \end{aligned}$$

Next, the contact forces at the centers of mass, defined by Eqs. (3) and (4), are then converted to joint torques using the Jacobian matrix. The resulting expression is as follows:

$$\tau_{Jh} = J_{hh}^T F_h + J_{kh}^T F_k \quad (6)$$

$$\tau_{Je} = -J_{he}^T F_h - J_{ke}^T F_k \quad (7)$$

where J_{hi} and J_{ki} denote the Jacobian matrices of the contact points.

3 Main Results

3.1 HTMO Design

Considering the uncertainties in human system modeling and the nonlinear, coupled effects in human-computer interaction, Eq. (1) of the human wear dynamics model can be revised as:

$$M_d(q_h)\ddot{q}_h + C_d(\dot{q}_h, q_h)\dot{q}_h + G_d(q_h) = \tau_{htotal} + \tau_{Jh} \quad (8)$$

where $M_d(q_h) = M_h(q_h) + \Delta M_h(q_h)$, $C_d(\dot{q}_h, q_h) = C_h(\dot{q}_h, q_h) + \Delta C_h(\dot{q}_h, q_h)$, $G_d(q_h) = G_h(q_h) + \Delta G_h(q_h)$, $\tau_{htotal} = \tau_h + \tau_d$, $\tau_{htotald} = \tau_{htotal} + \tau_{Jhd}$, τ_d is an unmodelled disturbance. M_d still satisfies the following properties[13]: 1) positive definite inertia matrix; 2) $\dot{M}_d(q) = C_d(q_h, \dot{q}_h) + C_d^T(q_h, \dot{q}_h)$.

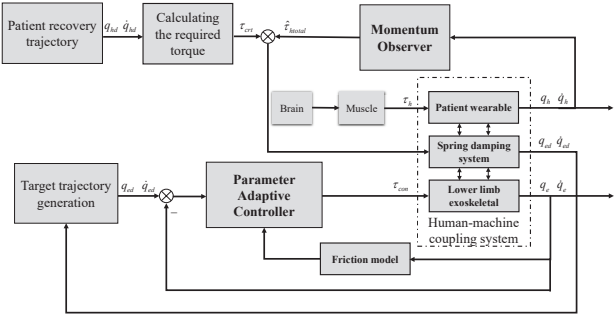


Fig. 2: System control logic block diagram

The definition of the human body's generalized momentum is as follows:

$$P = M_d \dot{q}_h \quad (9)$$

Take the time derivative of P :

$$\begin{aligned} \dot{P} &= \dot{M}_d \dot{q}_h + M_d \ddot{q}_h \\ &= \tau_{htotal} + \tau_{Jh} - G_d + C_d^T \dot{q}_h \end{aligned} \quad (10)$$

Inspired by [13]:

$$\dot{\hat{P}} = T_o + \tau_{Jh} - G_d + C_d^T \dot{q}_h \quad (11)$$

$$T_o = \ell(P - \hat{P}) \quad (12)$$

where T_o is called the residual vector. From Eq. (9)-(12), it follows that:

$$\dot{T}_o = \ell(\tau_{htotal} - T_o) \quad (13)$$

Next, a simultaneous Laplace transform on both sides of Eq. (13) is obtained:

$$\tau_{htotal}(s) = \frac{s + \ell}{\ell} T_o(s) \quad (14)$$

It can be seen that $\ell \rightarrow +\infty$, $T_o \rightarrow \tau_{htotal}$.

From Fig. 2, it can be concluded:

$$\tau_{crt} = \hat{\tau}_{htotal} + \tau_{Jhd} \quad (15)$$

where target interaction torque τ_{Jhd} is considered as assistance torque.

In an ideal scenario, when the patient has full voluntary control over their movements, the joint torque generated by the human body should satisfy the condition $\tau_{htotal} = \tau_{crt}$. However, most patients do not have full muscle control, i.e., $\tau_{htotal} < \tau_{crt}$, and the greater the difference between τ_{htotal} minus τ_{crt} , the greater the required assistive torque. Therefore, during the rehabilitation process, assistive control strategies can be implemented by adjusting the desired interaction torque to provide effective support and facilitate the recovery of motor functions, thereby offering appropriate assistance to the patient.

Based on Eq. (15), the desired target interaction torque τ_{Jhd} can be determined. Subsequently, the relationship between the interaction torque and the exoskeleton will be discussed. By deriving and transforming Eqs. (3) and (4) to (7), the following results can be obtained:

$$\tau_{Jhd} = J_{hh}^T (K_{\text{hint}} \begin{bmatrix} x_{e1d} - x_{h1} \\ y_{e1d} - y_{e1} \end{bmatrix} + D_{\text{hint}} \begin{bmatrix} \dot{x}_{e1d} - \dot{x}_{h1} \\ \dot{y}_{e1d} - \dot{y}_{h1} \end{bmatrix})$$

$$+ J_{hk}^T (K_{\text{kint}} \begin{bmatrix} x_{e2d} - x_{h2} \\ y_{e2d} - y_{h2} \end{bmatrix} + D_{\text{kint}} \begin{bmatrix} \dot{x}_{e2d} - \dot{x}_{h2} \\ \dot{y}_{e2d} - \dot{y}_{h2} \end{bmatrix}) \quad (16)$$

where (x_{e1d}, y_{e1d}) and (x_{e2d}, y_{e2d}) denote the target trajectories in the exoskeleton cartesian space. Substituting Eq. (7) into Eq. (16) and transforming it into angular space, we can simplify to obtain:

$$\begin{bmatrix} \dot{\theta}_{e1d} \\ \dot{\theta}_{e2d} \end{bmatrix} = \Gamma^{-1} \{ \tau_{Jhd} - [J_{hh}^T (K_{\text{hint}} \begin{bmatrix} x_{e1d} - x_{h1} \\ y_{e1d} - y_{e1} \end{bmatrix} - D_{\text{hint}} \begin{bmatrix} \dot{x}_{h1} \\ \dot{y}_{h1} \end{bmatrix}) + J_{hk}^T (K_{\text{kint}} \begin{bmatrix} x_{e2d} - x_{h2} \\ y_{e2d} - y_{h2} \end{bmatrix} + D_{\text{kint}} \begin{bmatrix} \dot{x}_{h2} \\ \dot{y}_{h2} \end{bmatrix})] \} \quad (17)$$

where $\Gamma = J_{hk}^T D_{\text{kint}} \begin{bmatrix} L_{e1d} C_{e1d} + l_{e2d} C_{e1de2d} l_{e2d} C_{e1de2d} \\ -L_{e1d} S_{e1d} - l_{e2d} S_{e1e2} - l_{e2d} S_{e1e2} \end{bmatrix} + J_{hh}^T D_{\text{hint}} \begin{bmatrix} l_{e1d} C_{e1d} & 0 \\ -l_{e1d} S_{e1d} & 0 \end{bmatrix}$, Therefore, it is only needed to integrate the matrix $\dot{q}_{ed} = [\dot{\theta}_{e1d} \ \dot{\theta}_{e2d}]^T$ to obtain the target tracking trajectory q_{ed} of the exoskeleton.

3.2 APC Design

Through the aforementioned analysis and discussion, the desired interaction torque has been effectively translated into the target trajectory of the exoskeleton. The subsequent steps will utilize the APC method to ensure accurate and rapid position tracking of the exoskeleton, thereby fulfilling the requirements for assisted rehabilitation. By combining Eqs. (1) and (7), the mathematical model of the exoskeleton is expressed as follows:

$$M_e(q_e) \ddot{q}_e + C_e(\dot{q}_e, q_e) \dot{q}_e + G_e(q_e) + \tau_f(\dot{q}_e) = u \quad (18)$$

where $u = \tau_{con} + \tau_{Je}$, τ_f and τ_{con} denote joint friction and controller input torque, respectively. In accordance with literature [16], τ_f is specifically expressed as follows:

$$\tau_f = (f_{cj} + (f_{sj} - f_{cj}) e^{-|\dot{\theta}_{ej}|^{\alpha}}) \text{sgn}(\dot{\theta}_{ej}) - f_{vj} \dot{\theta}_{ej} \quad (19)$$

where f_{cj} denotes the coulomb friction parameter, f_{sj} represents the static friction parameter, $\dot{\theta}_{ej}$ is the relative sliding velocity, θ_{js} is the stribbeck velocity, α is the exponential factor, and f_{vj} is the coefficient of viscous friction.

Based on the above dynamic equations, consider analyzing the system from the energy perspective: the kinetic and potential energy expressions are as follows:

$$\begin{aligned} E &= \frac{1}{2} \dot{q}_e^T M \dot{q}_e + m_{e1} g l_{e1} (1 - S_{e1}) \\ &+ m_{e2} g (1 - (l_{e1} S_{e1} + l_{e2} S_{e1e2})) \end{aligned} \quad (20)$$

Inspired by Eq. (20), the following error function on energy is designed:

$$\begin{aligned} V_E &= \frac{1}{2} \dot{q}_{err}^T M_e \dot{q}_{err} + m_{e1} g l_{e1} - S_{e1} \\ &+ m_{e2} g (1 - (l_{e1} S_{e1} + l_{e2} S_{e1e2})) \end{aligned} \quad (21)$$

where $\dot{q}_{err} = [\dot{\theta}_{e1}, \dot{\theta}_{e2}]^T$, $\dot{\theta}_{e1} = \dot{\theta}_{e1} - \dot{\theta}_{e1d}$, $\dot{\theta}_{e2} = \dot{\theta}_{e2} - \dot{\theta}_{e2d}$. Taking the time derivative of the energy equation E ,

the expression is as follows:

$$\begin{aligned}\dot{V}_E &= \dot{q}_{err}^T M_e \ddot{q}_{err} + \frac{1}{2} \dot{q}_{err}^T \dot{M}_e \dot{q}_{err} \\ &- (m_{e1} g l_{e1} C_{e1} + m_{e2} g l_{e1} C_{e1} + m_{e2} g l_{e2} C_{e1e2}) \dot{\theta}_{e1} \\ &- m_{e2} g l_{e2} C_{e1e2} \dot{\theta}_{e2}\end{aligned}\quad (22)$$

Substituting Eq. (18) into Eq. (22) and combining with $\dot{M}_e(\dot{q}_e) = C_e(\dot{q}_e, q_e) + C_e^T(\dot{q}_e, q_e)$, the expression is:

$$\begin{aligned}\dot{V}_E &= \dot{q}_{err}^T (u - C_e \dot{q}_e - G_e - \tau_f - M \ddot{q}_d + C_e(\dot{q}_e - \dot{q}_{ed})) \\ &- (m_{e1} g l_{e1} C_{e1} + m_{e2} g l_{e1} C_{e1} + m_{e2} g l_{e2} C_{e1e2}) \dot{\theta}_{e1} \\ &- m_{e2} g l_{e2} C_{e1e2} \dot{\theta}_{e2} \\ &= \dot{q}_{err}^T (u - \tau_f - M_e \ddot{q}_{ed} - C_e \dot{q}_{ed} - G_e) \\ &- (m_{e1} g l_{e1} C_{e1} + m_{e2} g l_{e1} C_{e1} + m_{e2} g l_{e2} C_{e1e2}) \dot{\theta}_{e1} \\ &- m_{e2} g l_{e2} C_{e1e2} \dot{\theta}_{e2} \\ &= \dot{q}_{err}^T (u - \tau_f - M_e \ddot{q}_{ed} - C_e \dot{q}_{ed}) \\ &+ (\dot{q}_e^T - \dot{q}_{ed}^T) \begin{bmatrix} G_{e1} \\ G_{e2} \end{bmatrix} + \dot{q}_e^T \begin{bmatrix} G_{e1} \\ G_{e2} \end{bmatrix} \\ &= \dot{q}_{err}^T (u - \tau_f - M_e \ddot{q}_{ed} - C_e \dot{q}_{ed}) + G_e \dot{q}_{ed}\end{aligned}\quad (23)$$

where $M_e \ddot{q}_{ed}$, $C_e \dot{q}_{ed}$ and τ_f are given below:

$$\begin{aligned}M_e \ddot{q}_{ed} &= \begin{bmatrix} n_1 + n_2 + 2n_3 C_{e2} & n_2 + n_3 C_{e2} \\ n_2 + n_3 C_{e2} & n_2 \end{bmatrix} \begin{bmatrix} \ddot{\theta}_{e1d} \\ \ddot{\theta}_{e2d} \end{bmatrix} \\ C_e \dot{q}_{ed} &= \begin{bmatrix} -2n_3 S_{e2} \dot{\theta}_{e2} & -n_3 S_{e2} \dot{\theta}_{e2} \\ n_3 S_{e2} \dot{\theta}_{e1} & 0 \end{bmatrix} \begin{bmatrix} \dot{\theta}_{e1d} \\ \dot{\theta}_{e2d} \end{bmatrix} \\ \tau_f &= \begin{bmatrix} n_4 \text{sgn}(\dot{\theta}_{e1}) - n_5 \dot{\theta}_{e1} \\ n_6 \text{sgn}(\dot{\theta}_{e2}) - n_7 \dot{\theta}_{e2} \end{bmatrix}\end{aligned}$$

and $n_1 = m_{e1} l_{e1}^2 + m_{e2} L_{e1}^2 + J_{e1}$; $n_2 = m_{e2} l_{e2}^2 + J_{e2}$; $n_3 = m_{e2} L_{e1} l_{e2}$, $n_4 = f_{c1} + (f_{s2} - f_{c2}) e^{-|\frac{\dot{\theta}_{2d}}{\theta_{2s}}|^\alpha}$; $n_5 = f_{v1}$; $n_6 = f_{c2} + (f_{s2} - f_{c2}) e^{-|\frac{\dot{\theta}_{2d}}{\theta_{2s}}|^\alpha}$; $n_7 = f_{v2}$.

Transform $M_e \ddot{q}_{ed} + C_e \dot{q}_{ed} + \tau_f$ in Eq. (23) into the following form:

$$M_e \ddot{q}_{ed} + C_e \dot{q}_{ed} + \tau_f = \begin{bmatrix} \psi_h^T \omega_h \\ \psi_k^T \omega_k \end{bmatrix} \quad (24)$$

where $\psi_h = [\psi_{h1} \psi_{h2} \psi_{h3} \psi_{h4} \psi_{h5}]^T$ and $\psi_k = [\psi_{k1} \psi_{k2} \psi_{k3} \psi_{k4}]^T$ denote the adaptive separation terms, and $\omega_h = [n_1 n_2 n_3 n_4 n_5]^T$ and $\omega_k = [n_2 n_3 n_6 n_7]^T$ represent time-varying parameters of the estimated system during motion. The specific separation expression is as follows:

$$\begin{aligned}\psi_{h1} &= \ddot{\theta}_{e1d}; \psi_{h2} = \ddot{\theta}_{e1d} + \ddot{\theta}_{e2d}; \\ \psi_{h3} &= 2C_{e2} \ddot{\theta}_{e1d} + C_{e2} \ddot{\theta}_{e2d} - 2S_{e2} \dot{\theta}_{e2} \dot{\theta}_{e1d} - S_{e2} \dot{\theta}_{e2} \dot{\theta}_{e2d}; \\ \psi_{h4} &= -\text{sgn}(\dot{\theta}_{e1}); \psi_{h5} = -\dot{\theta}_{e1}\end{aligned}\quad (25)$$

$$\begin{aligned}\psi_{k1} &= \ddot{\theta}_{1ed} + \ddot{\theta}_{e2d} \psi_{k2} = C_{e2} \ddot{\theta}_{e1d} + S_{e2} \dot{\theta}_{e1} \dot{\theta}_{e1d} \\ \psi_{k3} &= -\text{sgn}(\dot{\theta}_{e2}) \psi_{k4} = -\dot{\theta}_{e2}\end{aligned}\quad (26)$$

Bringing Eq. (24) into (23) simplifies to:

$$\dot{V}_E = (u_1 - \psi_h^T \omega_h) \dot{\theta}_{e1} + (u_2 - \psi_k^T \omega_k) \dot{\theta}_{e2} + G \dot{q}_{ed} \quad (27)$$

Due to the continuous variation of system parameters during the exoskeleton's motion and the limited accuracy of parameter identification, we estimate these parameters by introducing weighting factors w_1 and w_2 . Based on this, the following nonlinear controller is designed:

$$u_1 = -k_{ph} e_{\theta_1} - k_{dh} \dot{e}_{\theta_1} + \psi_h^T \hat{\omega}_h - G_{e1} \quad (28)$$

$$u_2 = -k_{pk} e_{\theta_2} - k_{dk} \dot{e}_{\theta_2} + \psi_k^T \hat{\omega}_k - G_{e2} \quad (29)$$

where $k_{ph}, k_{dh}, k_{pk}, k_{dk} \in R^+$ represent positive gain control parameters. $\hat{\omega}_h$ and $\hat{\omega}_k$ represent the estimated values of the uncertain vectors ω_h and ω_k , and their mathematical expressions are as follows:

$$\hat{\omega}_h = [\hat{n}_1 \ \hat{n}_2 \ \hat{n}_3 \ \hat{n}_4 \ \hat{n}_5]^T \quad (30)$$

$$\hat{\omega}_k = [\hat{n}_2 \ \hat{n}_3 \ \hat{n}_6 \ \hat{n}_7]^T \quad (31)$$

The parameter update rate is as follows:

$$\dot{\hat{\omega}}_h = -\Pi_h^{-1} \psi_h \dot{e}_{\theta_1} \quad (32)$$

$$\dot{\hat{\omega}}_k = -\Pi_k^{-1} \psi_k \dot{e}_{\theta_2} \quad (33)$$

where $\Pi_h = \text{diag}\{\Pi_{h1}, \dots, \Pi_{h5}\} \in R^+$ and $\Pi_k = \text{diag}\{\Pi_{k1}, \dots, \Pi_{k4}\} \in R^+$, and their parameters can be designed.

4 Simulation and discussion

4.1 Proposed controller

A mathematical model is built in Matlab/simulink to verify the effectiveness of the proposed control method. Where the target recovery trajectory is derived from literature [5] and optimised as follows:

$$\theta_{h1} = 90 - \sum_{i=1}^4 a_h[i] \sin(I\omega t) - \sum_{i=1}^4 b_h[i] \cos(I\omega t) + q_{h0} \quad (34)$$

$$\theta_{h2} = \sum_{i=1}^4 a_k[i] \sin(I\omega t) + \sum_{i=1}^4 b_k[i] \cos(I\omega t) + q_{k0} \quad (35)$$

where $\omega = 0.4\pi$, $a_{\varepsilon, hip}(\varepsilon = 1, \dots, 4)$ are -2.874, -2.423, 1.227, -0.1462, respectively, $b_{\varepsilon, hip}(\varepsilon = 1, \dots, 4)$ are 18.53, -2.016, -0.3704, 0.201 respectively, $a_{\varepsilon, knee}(\varepsilon = 1, \dots, 4)$ are 17.62, -2.469, -3.82, -0.1346 respectively, $b_{\varepsilon, knee}(\varepsilon = 1, \dots, 4)$ are -1.494, 11.72, 1.014, 0.2165 respectively, $q_{h0} = 10.07$ and $q_{k0} = -17.49$. The parameters of u are set as $k_{ph} = 500$, $k_{dh} = 50$, $k_{pk} = 100$, $k_{dk} = 25$, $\Pi_h = \text{diag}[10000 \ 10000 \ 1000 \ 100 \ 1000]$, $\Pi_k = \text{diag}[10 \ 10 \ 10 \ 10]$. The parameters of τ_f are set as $f_{cj} = 4.27$, $f_{sj} = 11.55$, $\theta_{js} = 107.17$, $f_{vj} = 0.067$, $\alpha = -1.38$. The specific system parameters are shown in **Table 2**.

To analyze the effectiveness of the APC when the wearer's lower limb mobility changes, τ_h is set to 35%, 70%, and 100% of the target input torque, simulating different levels of lower limb mobility of the wearer. $\tau_h = 35\% \tau_{Jhd}$, τ_h indicates that the wearer has varying degrees of lower limb muscle weakness. $\tau_h = 100\% \tau_{Jhd}$ indicates that the wearer has good lower limb health.

In Fig. 3, the estimated $\hat{\tau}_{htotal}$ of the HTMO is shown under different levels of the wearer's motion capabilities. According to the paper τ_{htotal} consists of τ_{htotal} and τ_{Jhd} , and

Table 2: System model parameters values

L_{h1} [m]	0.38	L_{e1} [m]	0.38	l_{h1} [m]	0.25
l_{e1} [m]	0.25	m_{h1} [kg]	8.171	m_{e1} [kg]	1.173
J_{h1} [kgm ²]	0.123	J_{e1} [kgm ²]	0.016	L_{h2} [m]	0.46
L_{e2} [m]	0.39	l_{h2} [m]	0.2	l_{e2} [m]	0.2
m_{h2} [kg]	3.859	m_{e2} [kg]	0.853	J_{h2} [kgm ²]	0.109
J_{e2} [kgm ²]	0.008	g [m/s ²]	9.8	K [N/m]	500
D [Ns/m]	1.25		-		-

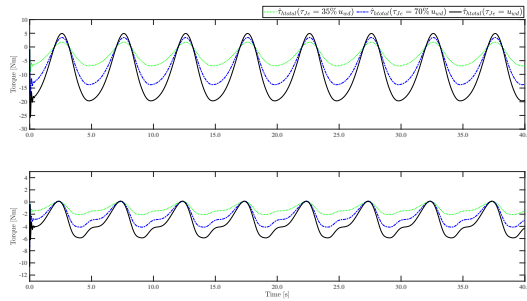


Fig. 3: HTMO when the human muscle moment is 35%, 70%, 100% of the target torque. upper: hip, lower: knee.

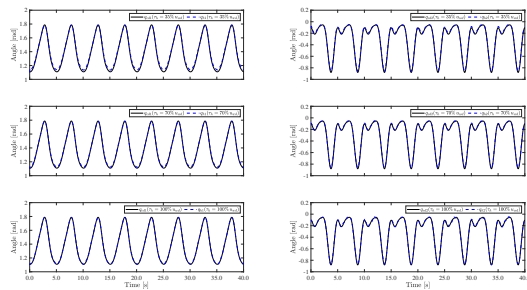


Fig. 4: Trajectory tracking chart of the wearer under different torques provided by the patient. left: hip, right: knee.

from Fig. 3, it can be seen that $\hat{\tau}_{htotal}$ approximates τ_h . The HMHO can qualitatively reflect the torque exerted by the patient. Then, $\tau_{htotal,d}$ is subtracted from $\hat{\tau}_{htotal}$, which can visualise the moment that the exoskeleton needs to provide. Additionally, the closer $\hat{\tau}_{htotal}$ is to $\tau_{htotal,d}$, the smaller the interactive force the exoskeleton needs to provide, indicating a stronger motion capability of the patient. Based on this, from Fig. 4, it can be seen that when the torque provided by the human body is 100% $\tau_{htotal,d}$, the errors in q_{ed} and q_h should be minimized. This also validates the relationship between the interaction torque and the target torque. It is worth mentioning that the exoskeleton trajectory q_{ed} is obtained from Eq. (17).

4.2 Contrast Controllers

In this section, the proposed controller is compared and analyzed with existing controllers (LQR, AANSMC). First, the linearized model is presented to prepare for the subsequent controller design:

$$M_e^* \ddot{q}_e + G_e^* = u \quad (36)$$

where $M_e^* = [m_{ij}^*] \in R^{2 \times 2}$. $i = 1, 2, j = 1, 2$. and $M_{e11}^* = m_2 L_1^2 + 2m_2 L_1 l_2 + m_1 l_1^2 + m_2 l_2^2 + J_1 + J_2$; $M_{e12}^* = M_{e21}^* = m_2 l_2^2 + L_1 m_2 l_2 + J_2$; $M_{e22}^* = m_2 l_2^2 + J_2$. $G_e^* = [G_{e1}^* \ G_{e2}^*]^T$, where $G_{e1}^* = -gl_2 m_2 - L_1 g m_2 - gl_1 m_1$; $G_{e2}^* = -gl_2 m_2$.

Then, the LQR[14] controller is designed as follows:

$$u_1^{lqr} = -k_{11}^l e_{\theta_1} - k_{12}^l e_{\theta_2} - k_{13}^l \dot{e}_{\theta_1} - k_{14}^l \dot{e}_{\theta_2} + \tau_{f1} \quad (37)$$

$$u_2^{lqr} = -k_{21}^l e_{\theta_1} - k_{22}^l e_{\theta_2} - k_{23}^l \dot{e}_{\theta_1} - k_{24}^l \dot{e}_{\theta_2} + \tau_{f2} \quad (38)$$

where τ_{f1} and τ_{f2} are friction compensation. By analysing the system, the parameters $Q = \text{diag}[2000 \ 2000 \ 2 \ 2]$ and $R = \text{diag}[0.1 \ 0.1]$ were selected to obtain the control parameters as follows: $k_{11}^l = 5458.8$, $k_{12}^l = 1.6$, $k_{13}^l = 0.51$, $k_{14}^l = 0.28$, $k_{21}^l = 0.15$, $k_{22}^l = 1045.3$, $k_{23}^l = -0.3$, $k_{24}^l = 0.75$.

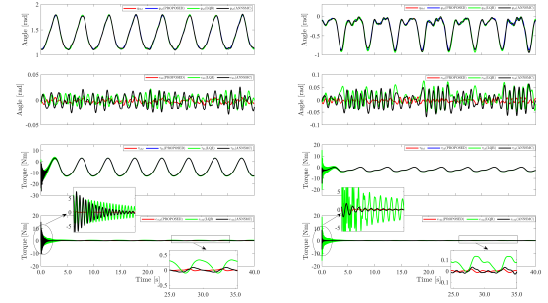


Fig. 5: Trajectory/interaction torque tracking curves under different controllers with 35% of patients providing torque. left: hip, right: knee.

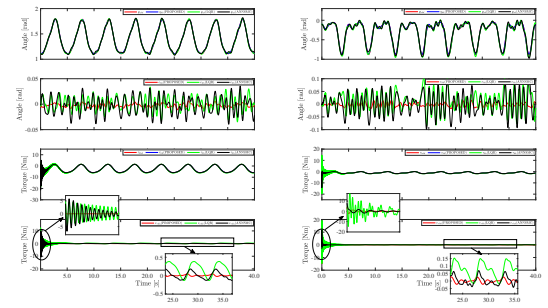


Fig. 6: Trajectory/interaction torque tracking curves under different controllers with 70% of patients providing torque. left: hip, right: knee.

The design of the second controller(AANSMC)[8] is as follows:

$$u = M_e (q_{ed} - K_v \dot{e}_{\theta} - K_p e_{\theta} - \rho \text{sgn} \dot{e}_{\theta}) + C_e \dot{q}_e + G_e \quad (39)$$

where $K_p = \text{diag}[850 \ 660]$, $K_v = \text{diag}[5 \ 20]$, $\rho = \text{diag}[0.5 \ 0.5]$.

From Fig. (5)-(7), the tracking errors between the rehabilitation motion trajectory and interaction torque under different torques provided by the patients are compared. A comparative analysis with LQR and AANSMC controls was conducted. The proposed control shows good performance in both the hip and knee joints. In the trajectory tracking of rehabilitation patients, the torque provided by the patient ranges from 35% to 100%, and the proposed controller's trajectory tracking error can always be controlled within 0.02

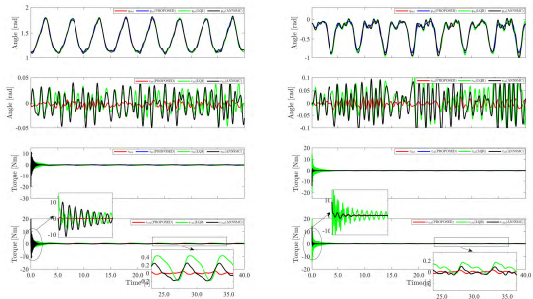


Fig. 7: Trajectory/interaction torque tracking curves under different controllers with 100% of patients providing torque. left: hip, right: knee.

rad. Compared with other controllers, LQR has an average of approximately 0.055 rad, while AANSMC is 0.5 rad. Additionally, in the interaction torque tracking system, whether in the initial tracking state (see the enlarged image) or the final steady state, compared to the severe oscillations of LQR and AANSMC, the proposed controller's torque output remains relatively smooth, ensuring the performance of the controller and the safety of the patient.

5 Conclusion

In this paper, we have proposed an innovative AAN control strategy for lower limb exoskeletons, aimed at enhancing rehabilitation outcomes. The approach integrates a human-machine coupling dynamics model, a HTMO, and APC, ensuring a dynamic and user-specific rehabilitation process. By effectively estimating joint torques and providing adaptive control, the system adjusts to varying patient conditions, offering personalized assistance. Simulation results demonstrate that the proposed strategy outperforms traditional controllers, including LQR and AANSMC, in terms of trajectory tracking accuracy and interaction torque smoothness. This approach not only minimizes tracking errors but also improves the safety and efficiency of rehabilitation, making it a promising solution for enhancing the therapeutic potential of exoskeleton-assisted rehabilitation.

References

- 1] Feigin V L, Brainin M, Norrving B, et al. World Stroke Organization (WSO): global stroke fact sheet 2022[J]. International Journal of Stroke, 2022, 17(1): 18-29.
- 2] Crocher V, Sahbani A, Robertson J, et al. Constraining upper limb synergies of hemiparetic patients using a robotic exoskeleton in the perspective of neuro-rehabilitation[J]. IEEE Transactions on Neural Systems and Rehabilitation Engineering, 2012, 20(3): 247-257.
- 3] Pérez-Ibarra JC, Siqueira AAG, Silva-Couto MA, et al. Adaptive impedance control applied to robot-aided neuro-rehabilitation of the ankle[J]. IEEE Robot Autom Lett 2019; 4(2): 185-92.
- 4] Vertechy R, Frisoli A, Dettori A, et al. Development of a new exoskeleton for upper limb rehabilitation[C]//2009 IEEE International Conference on Rehabilitation Robotics. IEEE, 2009: 188-193.
- 5] Wang Y, Wang H and Tian Y. Adaptive interaction torque-based AAN control for lower limb rehabilitation exoskeleton[J]. ISA Transactions 2022; 128: 184-197.

- [6] Murray SA, Ha KH, Hartigan C, et al. An assistive control approach for a lower-Limb exoskeleton to facilitate recovery of walking following stroke. IEEE Transactions on Neural Systems and Rehabilitation Engineering[J]. 2015; 23(3): 441-449.
- [7] Pehlivan A U, Losey P D, Malley M. Minimal Assist-as-Needed Controller for Upper Limb Robotic Rehabilitation. IEEE Transactions on Robotics[J]. A publication of the IEEE Robotics and Automation Society. 2016; 32(1): 113-124.
- [8] Chia E, Chang Y, Chang Y, et al. Assist-As-Needed rehabilitation using velocity field for upper limb exoskeleton[J]. Mechatronics. 2024; 97: 103115.
- [9] Luo L, Peng L, Wang C, et al. A Greedy Assist-as-Needed Controller for Upper Limb Rehabilitation[J]. IEEE Transactions on Neural Networks and Learning Systems. 2019; 30(11): 3433-3443.
- [10] Asl HJ, Katagiri K, Narikiyo T, et al. Satisfying Task Completion and Assist-As-Needed Performance in Robotic Exoskeletons[J]. IEEE Transactions on Medical Robotics and Bionics. 2021; 3(3): 791-800.
- [11] Teramae T, Noda T, Morimoto J. EMG-based model predictive control for physical human–robot interaction: Application for assist-as-needed control[J]. IEEE Robot Autom Lett. 2018; 3(1): 210–7.
- [12] Asl HJ, Narikiyo T, Kawanishi M. An assist-as-needed velocity field control scheme for rehabilitation robots[J]. In: IEEE int. conf. intell. robots syst. 2018.
- [13] Han L, Xu W, Li B, et al. Collision Detection and Coordinated Compliance Control for a Dual-Arm Robot Without Force/Torque Sensing Based on Momentum Observer[J]. IEEE/ASME Transactions on Mechatronics. 2019; 24(5): 2261-2272.
- [14] Scampicchio A, Aravkin A, Pillonetto G, Stable and robust LQR design via scenario approach. Automatica[J]. 2021; 129: 109571.
- [15] Tu Y, Zhu A, Song J, et al. An Adaptive Sliding Mode Variable Admittance Control Method for Lower Limb Rehabilitation Exoskeleton Robot[J]. Applied Sciences, 2020, 10(7):2536.
- [16] Ruderman M, Bertram T, Iwasaki M. Modeling, observation, and control of hysteresis torsion in elastic robot joints[J]. Mechatronics. 2014, 24(5): 407-415.